Symbolic Regression Methods for Reinforcement Learning

Jiří Kubalík, Jan Žegklitz, Erik Derner, and Robert Babuška

Abstract—**Reinforcement learning algorithms can be used to optimally solve dynamic decision-making and control problems. With continuous-valued state and input variables, reinforcement learning algorithms must rely on function approximators to represent the value function and policy mappings. Commonly used numerical approximators, such as neural networks or basis function expansions, have two main drawbacks: they are black-box models offering no insight in the mappings learned, and they require significant trial and error tuning of their meta-parameters. In this paper, we propose a new approach to constructing smooth value functions by means of symbolic regression. We introduce three off-line methods for finding value functions based on a state transition model: symbolic value iteration, symbolic policy iteration, and a direct solution of the Bellman equation. The methods are illustrated on four nonlinear control problems: velocity control under friction, one-link and two-link pendulum swing-up, and magnetic manipulation. The results show that the value functions not only yield well-performing policies, but also are compact, human-readable and mathematically tractable. This makes them potentially suitable for further analysis of the closed-loop system. A comparison with alternative approaches using neural networks shows that our method constructs well-performing value functions with substantially fewer parameters.**

Keywords—*reinforcement learning, value iteration, policy iteration, symbolic regression, genetic programming, nonlinear optimal control*

I. INTRODUCTION

Reinforcement learning (RL) in continuous-valued state and input spaces relies on function approximators. Various types of numerical approximators have been used to represent the value function and policy mappings: expansions with fixed or adaptive basis functions [1], [2], regression trees [3], local linear regression [4], [5], and deep neural networks [6]–[10].

The choice of a suitable approximator, in terms of its structure (number, type and distribution of the basis functions, number and size of layers in a neural network, etc.), is an ad hoc step which requires significant trial and error tuning.

The authors are with Czech Institute of Informatics, Robotics, and Cybernetics, Czech Technical University in Prague, Czech Republic, {jan.zegklitz, jiri.kubalik, erik.derner}@cvut.cz. Erik Derner is also with Department of Control Engineering, Faculty of Electrical Engineering, Czech Technical University in Prague, Czech Republic. Robert Babuška is also with Department of Cognitive Robotics, Delft University of Technology, The Netherlands, r.babuska@tudelft.nl.

There are no guidelines on how to design good value function approximator and, as a consequence, a large amount of expert knowledge and haphazard tuning is required when applying RL techniques to continuous-valued problems. In addition, these approximators are black box, yielding no insight and little possibility for analysis. Moreover, approaches based on deep neural networks often suffer from the lack of reproducibility, caused in large part by nondeterminism during the training process [11]. Finally, the interpolation properties of numerical function approximators may adversely affect the control performance and result in chattering control signals and steady-state errors [12]. In practice, this makes RL inferior to alternative control design methods, despite the theoretic potential of RL to produce optimal control policies.

To overcome these limitations, we propose a novel approach which uses symbolic regression (SR) to automatically construct an analytic representation of the value function. Symbolic regression has been used in nonlinear data-driven modeling with quite impressive results [13]–[16]. To our best knowledge, there have been no reports in the literature on the use of symbolic regression for constructing value functions. The closest related research is the use of genetic programming for fitting already available V-functions [17], [18], which, however, is completely different from our approach.

The paper is organized as follows. Section II describes the reinforcement learning framework considered in this work. Section III presents the proposed symbolic methods: symbolic value iteration, symbolic policy iteration, and a direct solution of the Bellman equation. In Section IV, we illustrate the working of these methods on a simple example: velocity control under nonlinear friction. Section V shows the experimental results on three nonlinear control problems: one-link and two-link pendulum swing-up and magnetic manipulation. Section VI concludes the paper.

II. RL FRAMEWORK

The dynamic system of interest is described by the state transition function

$$x_{k+1} = f(x_k, u_k) \tag{1}$$

with $x_k, x_{k+1} \in \mathcal{X} \subset \mathbb{R}^n$ and $u_k \in \mathcal{U} \subset \mathbb{R}^m$. Subscript k denotes discrete time instants. Function f is assumed to be given, but it does not have to be stated by explicit equations; it can be, for instance, a generative model given by a numerical simulation of complex differential equations. The control goal is specified through a *reward function* which assigns a scalar reward $r_{k+1} \in \mathbb{R}$ to each state transition from x_k to x_{k+1}:

$$r_{k+1} = \rho(x_k, u_k, x_{k+1}). \tag{2}$$

This function is defined by the user and typically calculates the reward based on the distance of the current state from a given reference (goal) state x_r to be attained. The state transition model and the associated reward function form the Markov decision process (MDP).

The goal of RL is to find an optimal control policy $\pi : \mathcal{X} \to \mathcal{U}$ such that in each state it selects a control action so that the cumulative discounted reward over time, called the return, is maximized:

$$R^\pi = E\Big\{ \sum_{k=0}^{\infty} \gamma^k \rho\big(x_k, \pi(x_k), x_{k+1}\big) \Big\} . \tag{3}$$

Here $\gamma \in (0, 1)$ is a discount factor and the initial state x_0 is drawn uniformly from the state space domain $\mathcal{X}$ or its subset. The return is approximated by the value function (V-function) $V^\pi : X \to \mathbb{R}$ defined as:

$$V^\pi(x) = E\Big\{ \sum_{k=0}^{\infty} \gamma^k \rho\big(x_k, \pi(x_k), x_{k+1}\big) \Big| x_0 = x \Big\} . \tag{4}$$

An approximation of the optimal V-function, denoted by $\hat{V}^*(x)$, can be computed by solving the Bellman optimality equation

$$\hat{V}^*(x) = \max_{u \in \mathcal{U}} \Big[\rho\big(x, \pi(x), f(x, u)\big) + \gamma \hat{V}^*\big(f(x, u)\big) \Big] . \tag{5}$$

To simplify the notation, in the sequel, we drop the hat and the star superscript: $V(x)$ will therefore denote the approximately optimal V-function. Based on $V(x)$, the optimal control action in any given state x is found as the one that maximizes the right-hand side of (5):

$$\pi(x) = \operatorname*{argmax}_{u \in \mathcal{U}} \big[\rho\big(x, u, f(x, u)\big) + \gamma V\big(f(x, u)\big) \big] \tag{6}$$

for all $x \in \mathcal{X}$.

In this paper, we use a RL framework based on V-functions. However, the proposed methods can be applied to Q-functions as well.

III. SOLVING BELLMAN EQUATION BY SYMBOLIC REGRESSION

We employ symbolic regression to construct an analytic approximation of the value function. Symbolic regression is a technique based on genetic programming and its purpose is to find an analytic equation describing given data. Our specific objective is to find an analytic equation for the value function that satisfies the Bellman optimality equation (5). Symbolic regression is a suitable technique for this task, as it does not rely on any prior knowledge on the form of the value function, which is generally unknown, and it has the potential to provide much more compact representations than, for instance, deep neural networks or basis function expansion models. In this work, we employ two different symbolic regression methods: a variant of Single Node Genetic Programming [19]–[22] and a variant of Multi-Gene Genetic Programming [23]–[25].

A. Symbolic regression

Symbolic regression is a suitable technique for this task, as we do not have to assume any detailed a priori knowledge on the structure of the nonlinear model. Symbolic regression methods were reported to perform better when using a linear combination of nonlinear functions found by means of genetic algorithms [26], [27]. Following this approach, we define the class of symbolic models as:

$$V(x) = \sum_{\iota}^{n_f} \beta_\iota \varphi_\iota(x) . \tag{7}$$

The nonlinear functions $\varphi_\iota(x)$, called features, are constructed by means of genetic programming using a predefined set of elementary functions $\mathcal{F}$ provided by the user. These functions can be nested and the SR algorithm evolves their combinations by using standard evolutionary operations such as mutation. The complexity of the symbolic models is constrained by two user-defined parameters: n_f, which is the number of features in the symbolic model, and δ, limiting the maximal depth of the tree representations of the nested functions. The coefficients β_ι are estimated by least squares, with or without regularization.

B. Data set

To apply symbolic regression, we first generate a set of n_x states sampled from $\mathcal{X}$:

$$X = \{x_1, \ldots, x_{n_x}\} \subset \mathcal{X},$$

and a set of n_u control inputs sampled from $\mathcal{U}$:

$$U = \{u_1, \ldots, u_{n_u}\} \subset \mathcal{U} .$$

The generic training data set for symbolic regression is then given by:

$$D = \{d_1, \ldots, d_{n_x}\} \tag{8}$$

with each training sample d_i being the tuple:

$$d_i = \langle x_i, x_{i,1}, r_{i,1}, \ldots, x_{i,n_u}, r_{i,n_u} \rangle$$

consisting of the state $x_i \in X$, all the next states $x_{i,j}$ obtained by applying in x_i all the control inputs $u_j \in U$ to the system model (1), and the corresponding rewards $r_{i,j} = \rho\big(x_i, u_j, f(x_i, u_j)\big)$.

In the sequel, V denotes the symbolic representation of the value function, generated by symbolic regression applied to data set D. We present three possible approaches to solving the Bellman equation by using symbolic regression.

C. Direct symbolic solution of Bellman equation

This approach directly evolves the symbolic value function so that it satisfies (5). The optimization criterion (fitness function) is the mean-squared error between the left-hand side and right-hand side of the Bellman equation, i.e., the Bellman error over all the training samples in D:

$$J^{\text{direct}} = \frac{1}{n_x} \sum_{i=1}^{n_x} \Big[\max_j \big(r_{i,j} + \gamma \underbrace{V(x_{i,j})}_{\text{evolved}} \big) - \underbrace{V(x_i)}_{\text{evolved}} \Big]^2 . \tag{9}$$

Unfortunately, the problem formulated in this way proved too hard to solve by symbolic regression, as illustrated later in Sections IV and V. We hypothesize that this difficulty stems from the fact that the fitness of the value function to be evolved is evaluated through the complex implicit relation in (9), which is not a standard regression problem. By modifying symbolic regression, the problem might be rendered feasible, but in this paper we successfully adopt an iterative approach, leading to the symbolic value iteration and symbolic policy iteration, as described below.

D. Symbolic value iteration

In symbolic value iteration (SVI), the optimal value function is found iteratively, just like in standard value iteration [28]. In each iteration ℓ, the value function $V_{\ell-1}$ from the previous iteration is used to compute the target for improving the value function V_ℓ in the current iteration. For each state $x_i \in X$, the target $t_{i,\ell} \in \mathbb{R}$ is calculated by evaluating the right-hand-side of (5):

$$t_{i,\ell} = \max_{u \in U} \Big(\rho(x_i, u, f(x_i, u)) + \gamma V_{\ell-1}\big(f(x_i, u)\big) \Big). \quad (10)$$

Here, the maximization is carried out over the predefined discrete control action set U. In principle, it would also be possible to use numerical or even symbolic optimization over the original continuous set $\mathcal{U}$. However, this is computationally more expensive, as the optimization problem would have to be solved n_x times at the beginning of each iteration. For this reason, we prefer the maximization over U, as stated in (10). In addition, as the next states and rewards are pre-computed and provided to the SVI algorithm in the data set D (8), we can replace (10) by its computationally more efficient equivalent:

$$t_{i,\ell} = \max_j \big(r_{i,j} + \gamma V_{\ell-1}(x_{i,j}) \big). \quad (11)$$

Given the target $t_{i,\ell}$, an improved value function V_ℓ is constructed by applying symbolic regression with the following fitness function:

$$J_\ell^{\text{SVI}} = \frac{1}{n_x} \sum_{i=1}^{n_x} \Big[\underbrace{t_{i,\ell}}_{\text{target}} - \underbrace{V_\ell(x_i)}_{\text{evolved}} \Big]^2. \quad (12)$$

This fitness function is again the mean-squared Bellman error. However, as opposed to (9), the above criterion (12) defines a true regression problem: the target to be fitted is fixed as it is based on $V_{\ell-1}$ from the previous iteration. In the first iteration, V_0 can be initialized either by some suitable function, or as $V_0(x) = 0$ for all $x \in \mathcal{X}$, in the absence of better initial value. In the latter case, the first target becomes the largest reward over all the next states.

In each iteration, the training data set for symbolic regression is composed as follows:

$$D_\ell^{\text{SVI}} = \{d_1, \ldots, d_{n_x}\} \text{ with } d_i = \langle x_i, t_{i,\ell} \rangle$$

i.e., each sample contains the state x_i, and the corresponding target $t_{i,\ell}$ computed by (11).

The SVI procedure terminates once a predefined maximum number of iterations n_i has been reached. Other stopping
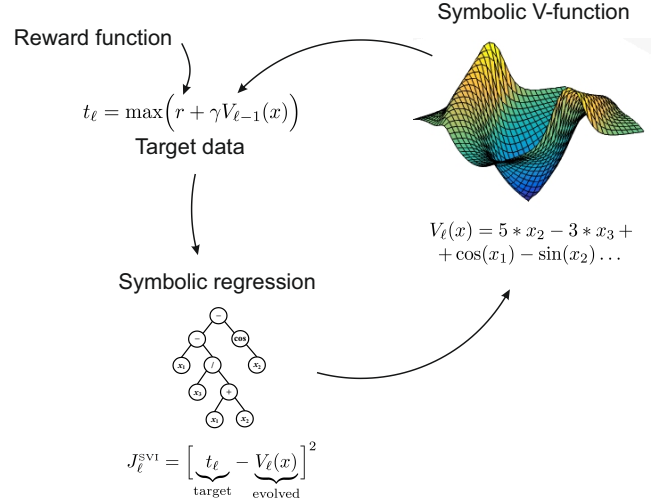

Fig. 1. Symbolic value iteration loop. In each iteration, the target data for symbolic regression are computed using the Bellman equation right-hand side. Symbolic regression then improves the value function and the process repeats.

criteria can be employed, such as terminating the iteration when the following condition is satisfied:

$$\max_i |V_\ell(x_i) - V_{\ell-1}(x_i)| \le \epsilon \quad (13)$$

with ϵ a user-defined convergence threshold. The resulting *symbolic value iteration* algorithm is given in Algorithm 1 and depicted in Figure 1. In each iteration, the symbolic regression algorithm is run for n_g generations.

Algorithm 1: Symbolic value iteration (SVI)

Input: training data set D, n_i
$\ell \leftarrow 0$, $V_0(x) = 0$, $\forall x \in \mathcal{X}$
while $\ell < n_i$ **do**
 $\quad \ell \leftarrow \ell + 1$
 $\quad \forall x_i \in X$ compute $t_{i,\ell}$ by using (11)
 $\quad D_\ell^{\text{SVI}} \leftarrow \{d_1, \ldots, d_{n_x}\}$ with $d_i = \langle x_i, t_{i,\ell} \rangle$
 $\quad V_\ell \leftarrow \text{SymbolicRegression}(D_\ell^{\text{SVI}}, J_\ell^{\text{SVI}})$
end
$V \leftarrow V_\ell$
Output: Symbolic value function V

E. Symbolic policy iteration

Also the symbolic policy iteration (SPI) algorithm iteratively improves the V-function estimate. However, rather than using $V_{\ell-1}$ to compute the target in each iteration, we derive from $V_{\ell-1}$ the currently optimal policy and plug it into the Bellman equation, so eliminating the maximum operator.

Given the value function $V_{\ell-1}$ from the previous iteration, for each state $x_i \in X$, the corresponding currently optimal

control action u_i^* is computed by:

$$u_i^* = \operatorname*{argmax}_{u \in U} \Big(\rho(x_i, u, f(x_i, u)) + \gamma V_{\ell-1}\big(f(x_i, u)\big) \Big), \quad (14)$$

$\forall x_i \in X$. Again, the maximization can be carried out over the original continuous set $\mathcal{U}$, rather than the discrete set U, which would incur higher computational costs.

Now, for each state x_i and the corresponding optimal control action u_i^*, the optimal next state x_i^* and the respective reward r_i^* can be computed:

$$x_i^* = f(x_i, u_i^*), \quad r_i^* = \rho(x_i, u_i^*, x_i^*). \quad (15)$$

As the next states and rewards are provided to the SPI algorithm in the data set D (8), we can replace (14) by its computationally more efficient equivalent. The index j^* of the optimal control action selected from U is found by:

$$j^* = \operatorname*{argmax}_{j} \big(r_{i,j} + \gamma V_{\ell-1}(x_{i,j}) \big), \quad (16)$$

$$x_i^* = x_{i,j^*}, \quad r_i^* = r_{i,j^*}. \quad (17)$$

with x_{i,j^*} and r_{i,j^*} selected from D. Given these samples, we can now construct the training data set for SR as follows:

$$D_\ell^{\mathrm{SPI}} = \{d_1, \ldots, d_{n_x}\} \text{ with } d_i = \langle x_i, x_i^*, r_i^* \rangle.$$

This means that each sample d_i contains the state x_i, the currently optimal next state x_i^* and the respective reward r_i^*. In each iteration ℓ of SPI, an improved approximation V_ℓ is sought by means of symbolic regression with the following fitness function:

$$J_\ell^{\mathrm{SPI}} = \frac{1}{n_x} \sum_{i=1}^{n_x} \Big(\underbrace{r_i^*}_{\text{target}} - [\underbrace{V_\ell(x_i)}_{\text{evolved}} - \gamma \underbrace{V_\ell(x_i^*)}_{\text{evolved}}] \Big)^2. \quad (18)$$

The fitness is again the mean-squared Bellman error, where only the currently optimal reward serves as the target for the difference $V_\ell(x_i) - \gamma V_\ell(x_i^*)$, with V_ℓ evolved by SR. The resulting *symbolic policy iteration* algorithm is given in Algorithm 2.

Algorithm 2: Symbolic policy iteration (SPI)

Input: training data set D, n_i
$\ell \leftarrow 0$, $V_0(x) = 0$, $\forall x \in \mathcal{X}$
while $\ell < n_i$ **do**
    $\ell \leftarrow \ell + 1$
    $\forall x_i \in X$ select x_i^* and r_i^* from D by (16) and (17)
    $D_\ell^{\mathrm{SPI}} \leftarrow \{d_1, \ldots, d_{n_x}\}$ with $d_i = \langle x_i, x_i^*, r_i^* \rangle$
    $V_\ell \leftarrow \mathrm{SymbolicRegression}(D_\ell^{\mathrm{SPI}}, J_\ell^{\mathrm{SPI}})$
end
$V \leftarrow V_\ell$
Output: Symbolic value function V

F. Performance measures for evaluating value functions

Note that the convergence of the iterative algorithms is not necessarily monotonic, similarly to other approximate solutions, like the fitted Q-iteration algorithm [3]. Therefore, it is not meaningful to retain only the last solution. Instead, we store the intermediate solutions from all iterations and use a posteriori analysis to select the best value function according to the performance measures described below.

Root mean squared Bellman error (BE) is calculated over all n_x state samples in the training data set D according to

$$\mathrm{BE} = \sqrt{\frac{1}{n_x} \sum_{i=1}^{n_x} \Big[\max_j \big(r_{i,j} + \gamma V(x_{i,j}) \big) - V(x_i) \Big]^2}.$$

In the optimal case, the Bellman error is equal to zero.

The following two measures are calculated based on closed-loop control simulations with the state transition model (1). The simulations start from n_s different initial states in the set X_{init} ($n_s = |X_{\mathrm{init}}|$) and run for a fixed amount of time T_{sim}. In each simulation time step, the optimal control action is computed according to the argmax policy (6).

Mean discounted return (R_γ) is calculated over the simulations from all the initial states in X_{init}:

$$R_\gamma = \frac{1}{n_s} \sum_{s=1}^{n_s} \sum_{k=0}^{T_{\mathrm{sim}}/T_s} \gamma^k \rho\big(x_k^{(s)}, \pi(x_k^{(s)}), x_{k+1}^{(s)} \big)$$

where (s) denotes the index of the simulation, $x_0^{(s)} \in X_{\mathrm{init}}$ and T_s is the sampling period. Larger values of R_γ indicate a better performance.

Percentage of successful simulations (S) within all n_s simulations. A simulation is considered successful if the state x stays within a predefined neighborhood of the goal state for the last T_{end} seconds of the simulation. Generally, the neighborhood $N(x_r)$ of the goal state in n-dimensional state space is defined using a neighborhood size parameter $\varepsilon \in \mathbb{R}^n$ as follows:

$$N(x_r) = \{x : |x_{r,i} - x_i| \le \varepsilon_i, \text{ for } i = 1 \ldots n\}.$$

Larger values of S correspond to a better performance.

G. Experimental evaluation scheme

Each of the three proposed approaches (direct, SVI, and SPI) was implemented in two variants, one using the Single Node Genetic Programming (SNGP) algorithm and the other one using the Multi-Gene Genetic Programming (MGGP) algorithm. A detailed explanation of the SR algorithms and their parameters is beyond the scope of this paper and we refer the interested reader for more details on the implementation of SNGP to [22] and for MGGP to [25].

There are six algorithms in total to be tested: `direct-SNGP`, `direct-MGGP`, `SPI-SNGP`, `SPI-MGGP`, `SVI-SNGP` and `SVI-MGGP`. Note, however, that our goal

is not to compare the two symbolic regression algorithms. Instead, we want to demonstrate that the proposed symbolic RL methods are general and can be implemented by using more than one specific symbolic regression algorithm.

Each of the algorithms was run $n_r = 30$ times with the same parameters, but with a different randomization seed. Each run delivers three winning V-functions, which are the best ones with respect to R_γ, BE and S, respectively. Statistics such as the median, min, and max calculated over the set of n_r respective winner V-functions are used as performance measures of the particular method (SVI, SPI and direct) and the SR algorithm (SNGP, MGGP). For instance, the median of S is calculated as

$$\operatorname*{med}_{r=1..n_r} (\operatorname*{max}_{i=1..n_i} (S_{r,i})) \qquad (19)$$

where $S_{r,i}$ denotes the percentage of successful simulations in iteration i of run r. For the direct method, the above maximum is calculated over all generations of the SR run.

For comparison purposes, we have calculated a baseline solution, which is a numerical V-function approximation calculated by the fuzzy V-iteration algorithm [29] with triangular basis functions.

IV. Illustrative example

We start by illustrating the working of the proposed methods on a practically relevant first-order, nonlinear motion-control problem. Many applications require high-precision position and velocity control, which is often hampered by the presence of friction. Without proper nonlinear compensation, friction causes significant tracking errors, stick-slip motion and limit cycles. To address these problems, we design a nonlinear velocity controller for a DC motor with friction by using the proposed symbolic methods.

The continuous-time system dynamics are given by:

$$I\dot{v}(t) + (b + \frac{K^2}{R})v(t) + F_c\big(v(t), u(t), c\big) = \frac{K}{R}u(t) \qquad (20)$$

with $v(t)$ and $\dot{v}(t)$ the angular velocity and acceleration, respectively. The angular velocity varies in the interval $[-10, 10]\,\text{rad·s}^{-1}$. The control input $u \in [-4, 4]\,\text{V}$ is the voltage applied to the DC motor and the parameters of the system are: moment of inertia $I = 1.8 \times 10^{-4}\,\text{kg·m}^2$, viscous friction coefficient $b = 1.9 \times 10^{-5}\,\text{N·m·s·rad}^{-1}$, motor constant $K = 0.0536\,\text{N·m·A}^{-1}$, armature resistance $R = 9.5\,\Omega$, and Coulomb friction coefficient $c = 8.5 \times 10^{-3}\,\text{N·m}$.

The Coulomb friction force F_c is modeled as [30]:

$$F_c\big(v(t), u(t), c\big) =$$
$$\begin{cases} c & \text{if } v(t) > 0 \text{ or } v(t) = 0 \text{ and } u(t) > c\frac{R}{K} \\ -c & \text{if } v(t) < 0 \text{ or } v(t) = 0 \text{ and } u(t) < -c\frac{R}{K} \\ \frac{K}{R}u(t) & \text{if } v(t) = 0 \text{ and } \left|\frac{K}{R}u(t)\right| \leq c \end{cases}$$

The discrete-time transitions are obtained by numerically integrating the continuous-time dynamics using the fourth-order Runge-Kutta method and a sampling period $T_s = 0.001\,\text{s}$. The

state is the velocity, $x = v$, and the reward function is defined as:

$$r_{k+1} = \rho(x_k, u_k, x_{k+1}) = \sqrt{|x_r - x_k|} \qquad (21)$$

with $x_r = 7\,\text{rad·s}^{-1}$ the desired velocity (goal state).

The symbolic regression parameters are listed in Table VIII. The number in parentheses in the first row refers to SPI, which converges faster and needs fewer iterations. The parameters for the direct method are identical, except for the number of generations, which was 50 000 in total (the method does not iterate). We chose the elementary function set to be $\mathcal{F} = \{*, +, -, \text{square, cube, bent identity}^1\}$ for all methods. The same function set was used also for all the experiments reported in Section V.

The parameters of the experiment are listed in Table VII. In each of the 30 runs, we selected the best V-function with respect to S. Figure 2 shows the median values of S calculated for the V-functions over all 30 runs by using equation (19). The SVI method is consistently the best one, followed by SPI and direct.
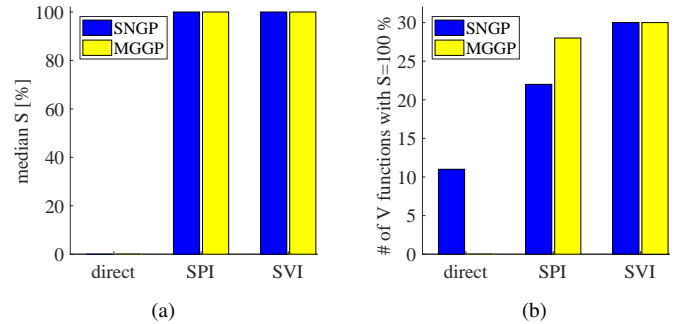

Fig. 2. Performance on the friction compensation problem: (a) median percentage of successful simulations S, (b) the number of runs in which a V-function with S=100 % was found.

The performance measures R_γ, BE and S are listed in Table I. For the S measure, the first two numbers in the square brackets are the minimum and maximum value and the number in parentheses is the frequency of the value. Interestingly, we found that low BE does not necessarily correlate with high performance of the V-function in the control task.

TABLE I. Performance of the symbolic methods on the friction problem. The performance of the baseline V-function is $R_\gamma = -42.158$, $BE = 1.7 \times 10^{-5}$, $S = 100\,\%$.

SNGP	direct	SPI	SVI
R_γ [–]	-48.184	-42.563	-42.339
BE [–]	0.301	0.0212	2.571
S [%]	0	100	100
	[0, 100 (11)]	[0, 100 (22)]	[100, 100 (30)]
MGGP	direct	SPI	SVI
R_γ [–]	-48.184	-42.565	-42.274
BE [–]	0.719	1.552	2.619
S [%]	0	100	100
	[0, 0 (30)]	[0, 100 (28)]	[100, 100 (30)]

Figure 3 shows examples of well-performing symbolic V-functions found through symbolic regression, compared to

---

[1] https://en.wikipedia.org/wiki/Bent_function

a baseline V-function calculated using the numerical approximator [29]. A closed-loop simulation is presented in Figure 4. Both the symbolic and baseline V-function yield optimal performance.

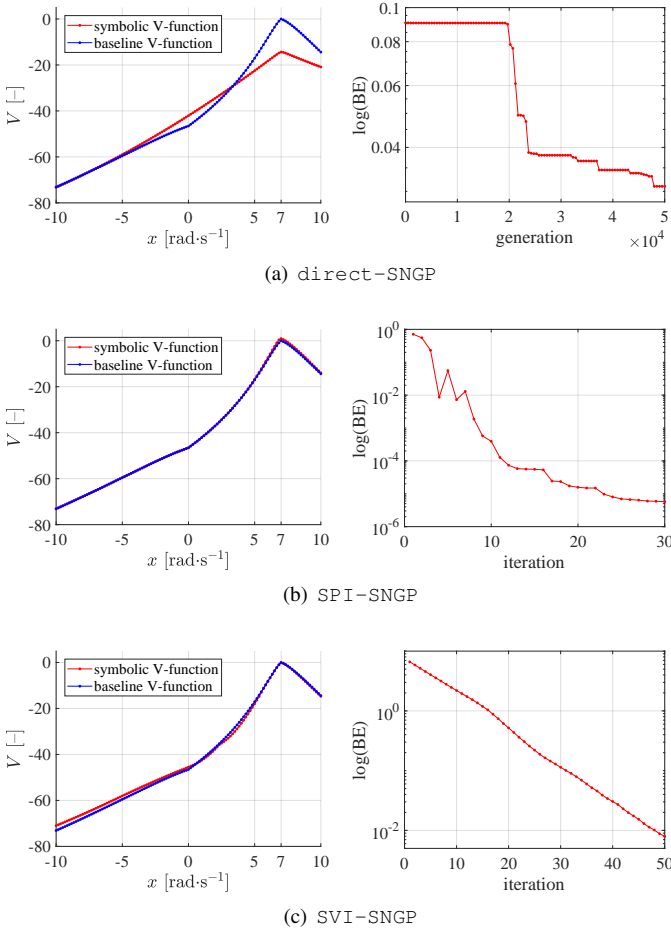(a) direct-SNGP

(b) SPI-SNGP

(c) SVI-SNGP

Fig. 3. Examples of typical well-performing V-functions found for the friction compensation problem. Left: the symbolic V-function compared to the baseline. Right: the Bellman error.

The proposed symbolic methods reliably find well-performing V-functions for the friction compensation problem. Interestingly, even the direct approach can solve this problem when using the SNGP algorithm. However, it finds a well-performing V-function with respect to S only in approximately one third of the runs.

V. EXPERIMENTS

In this section, experiments are reported for three non-linear control problems: 1-DOF and 2-DOF pendulum swing-up, and magnetic manipulation. The parameters of these experiments are listed in Table VII.

A. 1-DOF pendulum swing-up

The inverted pendulum (denoted as 1DOF) consists of a weight of mass m attached to an actuated link that rotates
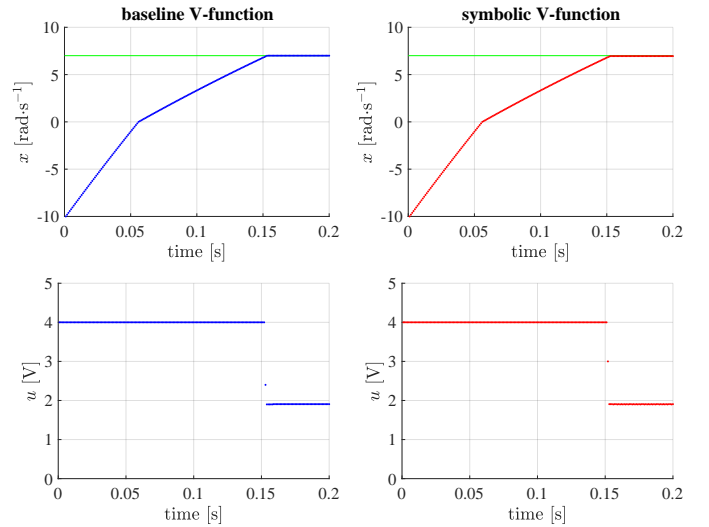

Fig. 4. Simulations of the friction compensation problem with the baseline V-function (left) and the symbolic V-function (right) presented in Figure 3b). The upper plots show the state trajectory from $x_0 = -10 \, \mathrm{rad \cdot s^{-1}}$. The lower plots show the corresponding control inputs. Only the first $0.2 \, \mathrm{s}$ of the simulation are shown as the variables remain constant afterwards.

in a vertical plane. The available torque is insufficient to push the pendulum up in a single rotation from many initial states. Instead, from certain states (e.g., when the pendulum is pointing down), it needs to be swung back and forth to gather energy, prior to being pushed up and stabilized. The continuous-time model of the pendulum dynamics is:

$$\ddot{\alpha} = \frac{1}{I} \cdot \left[mgl \sin(\alpha) - b\dot{\alpha} - \frac{K^2}{R}\dot{\alpha} + \frac{K}{R}u \right] \quad (22)$$

where $I = 1.91 \times 10^{-4} \, \mathrm{kg \cdot m^2}$, $m = 0.055 \, \mathrm{kg}$, $g = 9.81 \, \mathrm{m \cdot s^{-2}}$, $l = 0.042 \, \mathrm{m}$, $b = 3 \times 10^{-6} \, \mathrm{N \cdot m \cdot s \cdot rad^{-1}}$, $K = 0.0536 \, \mathrm{N \cdot m \cdot A^{-1}}$, $R = 9.5 \, \Omega$. The angle α varies in the interval $[-\pi, \pi] \, \mathrm{rad}$, with $\alpha = 0 \, \mathrm{rad}$ pointing up, and 'wraps around' so that e.g. a rotation of $3\pi/2 \, \mathrm{rad}$ corresponds to $\alpha = -\pi/2 \, \mathrm{rad}$. The state vector is $x = [\alpha, \dot{\alpha}]^\top$. The sampling period is $T_s = 0.05 \, \mathrm{s}$, and the discrete-time transitions are obtained by numerically integrating the continuous-time dynamics (22) by using the fourth-order Runge-Kutta method. The control input u is limited to $[-2, 2] \, \mathrm{V}$, which is insufficient to push the pendulum up in one go.

The control goal is to stabilize the pendulum in the unstable equilibrium $\alpha = \dot{\alpha} = 0$, which is expressed by the following reward function:

$$\rho(x, u, f(x, u)) = -|x|^\top Q \quad (23)$$

with $Q = [1, 0]^\top$ a weighting vector to adjust the relative importance of the angle and angular velocity.

The symbolic regression parameters are listed in Table VIII. The statistical results obtained from 30 independent runs are presented in Figure 5 and Table II.

Figure 5 shows that the SVI and SPI methods achieve comparable performance, while the direct method fails.
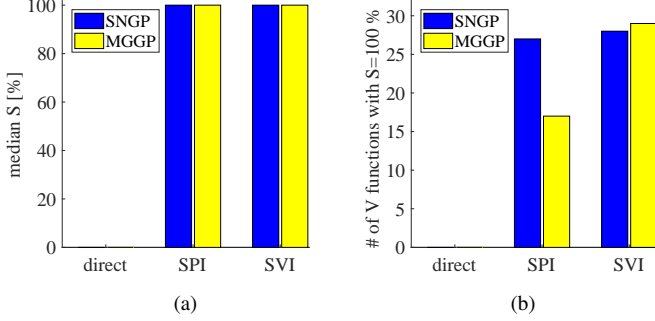
Fig. 5. Performance on the 1DOF problem: (a) median S, (b) the number of runs in which a V-function with S=100% was found.

TABLE II. PERFORMANCE OF THE SYMBOLIC METHODS ON THE 1DOF PROBLEM. THE PERFORMANCE OF THE BASELINE V-FUNCTION IS $R_\gamma = -9.346$, BE = 0.0174, S = 100%.

SNGP	direct	SPI	SVI
R_γ [–]	-26.083	-10.187	-10.013
BE [–]	0.478	0.242	0.615
S [%]	0	100	100
	[0, 0 (30)]	[81.3, 100 (27)]	[93.8, 100 (28)]
MGGP	direct	SPI	SVI
R_γ [–]	-26.083	-10.487	-9.917
BE [–]	0.776	0.797	0.623
S [%]	0	100	100
	[0, 6.25 (2)]	[0, 100 (17)]	[0, 100 (29)]

An example of a well-performing symbolic V-function found through symbolic regression, compared to a baseline V-function calculated using the numerical approximator [29], is shown in Figure 6. The symbolic V-function is smoother than the numerical baseline, which can be seen on the level curves and on the state trajectory. The difference is particularly notable in the vicinity of the goal state, which is a significant advantage of the proposed method.

A simulation with the symbolic V-function, as well as an experiment with the real system [5], is presented in Figure 7. The trajectory of the control signal u on the real system shows the typical bang-bang nature of optimal control, which illustrates that symbolic regression found a near optimal value function.

The symbolic V-function depicted in Figure 6, constructed by the `SVI-SNGP` method, has the following form:

$$
\begin{aligned}
V(x) &= 1.7 \times 10^{-5}(10x_2 - 12x_1 + 47)(4.3 \times 10^{-2}x_2 - 3.5x_1 + 11)^3 \\
&- 7.1 \times 10^{-4}x_2 - 4.6x_1 - 8.2 \times 10^{-6}(4.3 \times 10^{-2}x_2 - 3.5x_1 \\
&+ 11)^3(0.2x_1 + 0.3x_2 - 0.5)^3 - 9.8 \times 10^{-3}(0.4x_1 + 0.1x_2 - 1.1)^6 \\
&+ 11(0.1x_1 - 1.5)^3 + 11((0.6x_1 + 6.3 \times 10^{-2}x_2 - 1.7)^2 + 1)^{0.5} \\
&+ 8.7 \times 10^{-6}((10x_2 - 12x_1 + 47)^2(4.3 \times 10^{-2}x_2 - 3.5x_1 + 11)^6 + 1)^{0.5} \\
&+ 0.3((1.1x_1 + 0.4x_2 - 3.3)^2 + 1)^{0.5} + (3.9 \times 10^{-3}(4.3 \times 10^{-2}x_2 \\
&- 3.5x_1 + 11)^2(0.2x_1 + 0.3x_2 - 0.5)^2 + 1)^{0.5} + 6.5 \times 10^{-5}((1.2x_1 \\
&+ 14x_2 - 10)^2(9.1 \times 10^{-2}x_2 - 2.9x_1 + 0.5((9.1 \times 10^{-2}x_2 - 2.9x_1 \\
&+ 8.3)^2 + 1)^{0.5} + 7.8)^2 + 1)^{0.5} - 5.5 \times 10^{-2}(4.3 \times 10^{-2}x_2 \\
&- 3.5x_1 + 11)(0.2x_1 + 0.3x_2 - 0.5) - 1.7((3.6x_1 + 0.4x_2 - 11)^2 + 1)^{0.5} \\
&- 2((x_1 - 3.1)^2 + 1)^{0.5} - 1.3 \times 10^{-4}(1.2x_1 + 14x_2 - 10)(9.1 \times 10^{-2}x_2 \\
&- 2.9x_1 + 0.5((9.1 \times 10^{-2}x_2 - 2.9x_1 + 8.3)^2 + 1)^{0.5} + 7.8) + 23 \,.
\end{aligned}
\tag{24}
$$

The example shows that symbolic V-functions are compact, analytically tractable and easy to plug into other algorithms. The number of parameters in the example is 100.

We have compared our results with an alternative approach using neural networks in the actor-critic scheme. The number of parameters needed is 122101 for a deep neural network DDPG [9] and 3791 for a smaller neural network used in [31]. Therefore, the number of parameters needed by the proposed method is significantly lower.

B. 2-DOF swing-up

The double pendulum (denoted as 2DOF) is described by the following continuous-time fourth-order nonlinear model:

$$M(\alpha)\ddot{\alpha} + C(\alpha, \dot{\alpha})\alpha + G(\alpha) = u \tag{25}$$

with $\alpha = [\alpha_1, \alpha_2]^\top$ the angular positions of the two links, $u = [u_1, u_2]^\top$ the control input, which are the torques of the two motors, $M(\alpha)$ the mass matrix, $C(\alpha, \dot{\alpha})$ the Coriolis and centrifugal forces matrix and $G(\alpha)$ the gravitational forces vector. The state vector x contains the angles and angular velocities and is defined by $x = [\alpha_1, \dot{\alpha_1}, \alpha_2, \dot{\alpha_2}]^\top$. The angles α_1, α_2 vary in the interval $[-\pi, \pi)$ rad and wrap around. The angular velocities $\dot{\alpha_1}$, $\dot{\alpha_2}$ are restricted to the interval $[-2\pi, 2\pi)$ rad·s^{-1} using saturation. Matrices $M(\alpha)$, $C(\alpha, \dot{\alpha})$ and $G(\alpha)$ are defined by:

$$
\begin{aligned}
M(\alpha) &= \begin{bmatrix} P_1 + P_2 + 2P_3 \cos(\alpha_2) & P_2 + P_3 \cos(\alpha_2) \\ P_2 + P_3 \cos(\alpha_2) & P_2 \end{bmatrix} \\
C(\alpha, \dot{\alpha}) &= \begin{bmatrix} b_1 - P_3\dot{\alpha_2}\sin(\alpha_2) & -P_3(\dot{\alpha_1} + \dot{\alpha_2})\sin(\alpha_2) \\ P_3\dot{\alpha_1}\sin(\alpha_2) & b_2 \end{bmatrix} \\
G(\alpha) &= \begin{bmatrix} -F_1 \sin(\alpha_1) - F_2 \sin(\alpha_1 + \alpha_2) \\ -F_2 \sin(\alpha_1 + \alpha_2) \end{bmatrix}
\end{aligned}
\tag{26}
$$

with $P_1 = m_1c_1^2 + m_2l_1^2 + I_1$, $P_2 = m_2c_2^2 + I_2$, $P_3 = m_2l_1c_2$, $F_1 = (m_1c_1 + m_2l_2)g$ and $F_2 = m_2c_2g$. The meaning and values of the system parameters are given in Table III. The transition function $f(x, u)$ is obtained by numerically integrating (25) between discrete time samples using the fourth-order Runge-Kutta method with the sampling period $T_s = 0.01$ s.

TABLE III. DOUBLE PENDULUM PARAMETERS

Model parameter	Symbol	Value	Unit
Link lengths	l_1, l_2	0.4, 0.4	m
Link masses	m_1, m_2	1.25, 0.8	kg
Link inertias	I_1, I_2	0.0667, 0.0427	kg·m^2
Center of mass coordinates	c_1, c_2	0.2, 0.2	m
Damping in the joints	b_1, b_2	0.08, 0.02	kg·s^{-1}
Gravitational acceleration	g	9.8	m·s^{-2}

The control goal is to stabilize the two links in the upper equilibrium, which is expressed by the following quadratic reward function:
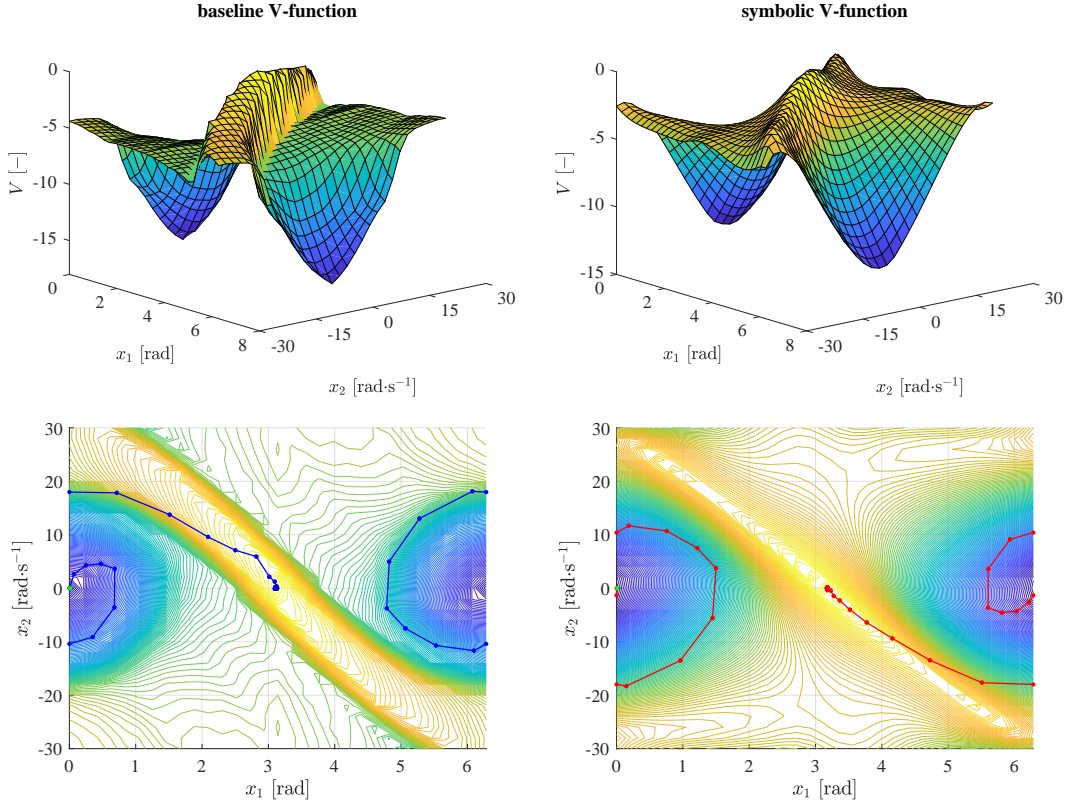
$$\rho(x, u, f(x, u)) = -|x|Q \tag{27}$$

baseline V-function   **symbolic V-function**

Fig. 6. Baseline and symbolic V-function produced by the `SVI-SNGP` method on the 1DOF problem. The symbolic V-function is smoother than the numerical baseline V-function, which can be seen on the level curves and on the state trajectory, in particular near the goal state.
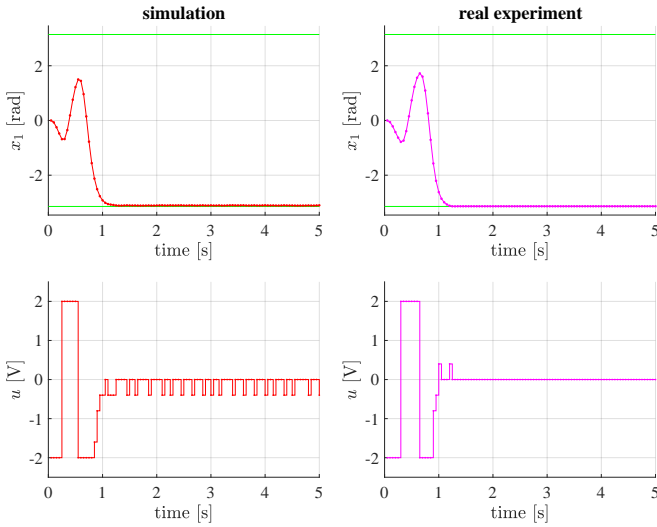
where $Q = [1, 0, 1.2, 0]^\top$ is a weighting vector to specify the relative importance of the angles and angular velocities.

The symbolic regression parameters are listed in Table VIII. The statistical results obtained from 30 independent runs are presented in Figure 8 and Table IV.
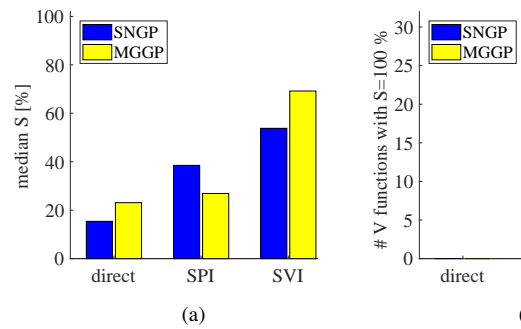

(a)   (b)

Fig. 8. Performance on the 2DOF problem: a) median S, b) the number of runs, out of 30, in which a V-function achieving S=100 % was found.

simulation   **real experiment**

Fig. 7. An example of a well-performing symbolic V-function found with the `SVI-SNGP` method on the 1DOF problem, used in a simulation (left) and on the real system (right). The performance of the SVI method is near-optimal even in the real experiment.

C. Magnetic manipulation

The magnetic manipulation (denoted as Magman) has several advantages compared to traditional robotic manipulation

TABLE IV.   RESULTS OBTAINED ON THE 2DOF PROBLEM. THE
PERFORMANCE OF THE BASELINE V-FUNCTION IS $R_\gamma = -80.884$,
$BE = 8 \times 10^{-6}$, S = 23 %.

SNGP	direct	SPI	SVI
R_γ [–]	−89.243	−85.607	−81.817
BE [–]	4.23	2.00	5.79
S [%]	15.4	38.5	53.8
	[7.7, 23.1 (14)]	[0, 100 (4)]	[7.7, 100 (4)]
MGGP	direct	SPI	SVI
R_γ [–]	−84.739	−84.116	−82.662
BE [–]	5.19	1.98	3.29
S [%]	23.1	26.9	69.2
	[0, 30.8 (1)]	[0, 100 (5)]	[7.7, 100 (2)]

approaches. It is contactless, which opens new possibilities for actuation on a micro scale and in environments where it is not possible to use traditional actuators. In addition, magnetic manipulation is not constrained by the robot arm morphology, and it is less constrained by obstacles.

A schematic of a magnetic manipulation setup [32] with two coils is shown in Figure 9. The two electromagnets are positioned at 0.025 m and 0.05 m. The current through the electromagnet coils is controlled to dynamically shape the magnetic field above the magnets and so to position a steel ball, which freely rolls on a rail, accurately and quickly to the desired set point.
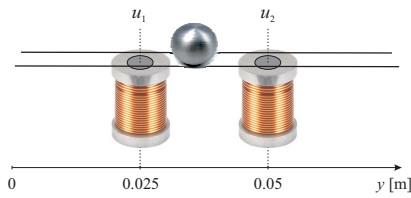

Fig. 9.   Magman schematic.

The horizontal acceleration of the ball is given by:

$$\ddot{y} = -\frac{b}{m}\dot{y} + \frac{1}{m}\sum_{i=1}^{2} g(y,i)\, u_i \qquad (28)$$

with

$$g(y,i) = \frac{-c_1\,(y - 0.025i)}{\left((y - 0.025i)^2 + c_2\right)^3}. \qquad (29)$$

Here, y denotes the position of the ball, $\dot{y}$ its velocity and $\ddot{y}$ the acceleration. With u_i the current through coil i, $g(y,i)$ is the nonlinear magnetic force equation, m the ball mass, and b the viscous friction of the ball on the rail. The model parameters are listed in Table V.

TABLE V.   MAGNETIC MANIPULATION SYSTEM PARAMETERS

Model parameter	Symbol	Value	Unit
Ball mass	m	3.200×10^{-2}	kg
Viscous damping	b	1.613×10^{-2}	N·s·m^{-1}
Empirical parameter	c_1	5.520×10^{-10}	N·m^5·A^{-1}
Empirical parameter	c_2	1.750×10^{-4}	m^2

State x is given by the position and velocity of the ball. The reward function is defined by:

$$\rho(x,u,f(x,u)) = -|x_r - x|Q, \text{ with } Q = \text{diag}[5,0]. \qquad (30)$$

The symbolic regression parameters are listed in Table VIII. The statistical results obtained from 30 independent runs are presented in Figure 10 and Table VI. An example of a well-performing symbolic V-function found through symbolic regression, compared to the baseline V-function calculated using the numerical approximator [29], is shown in Figure 11. A simulation with a symbolic and a baseline V-function is presented in Figure 12.

The symbolic V-function is smoother than the numerical baseline V-function and it performs well in the simulation. Nevertheless, the way of approaching the goal state is suboptimal when using the symbolic V-function. This result demonstrates the tradeoff between the complexity and the smoothness of the V-function.
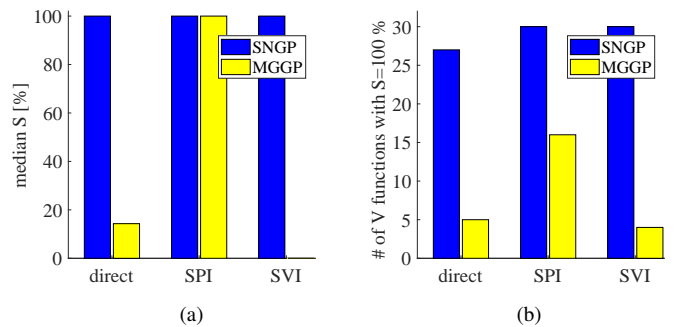

Fig. 10.   Performance on the Magman problem: a) median S, b) the number of runs, out of 30, in which a V-function achieving S=100 % was found.

TABLE VI.   RESULTS OBTAINED ON THE MAGMAN PROBLEM. THE
PERFORMANCE OF THE BASELINE V-FUNCTION IS $R_\gamma = -0.0097$,
$BE = 1.87 \times 10^{-4}$, S = 100 %.

SNGP	direct	SPI	SVI
R_γ	−9.917	−0.010	−0.011
BE	0.623	0.084	0.00298
S	100	100	100
	[7.14, 100 (27)]	[100, 100 (30)]	[100, 100 (30)]
MGGP	direct	SPI	SVI
R_γ	−0.164	−0.010	−0.169
BE	0.004	15.74	0.061
S	14.3	100	0
	[0, 100 (5)]	[0, 100 (16)]	[0, 100 (4)]

Similarly as in the 1DOF example, we have compared our results with an approach using neural networks in the actor-critic scheme. The number of parameters needed is 123001 for a deep neural network DDPG [9] and 3941 for a neural network used in [31]. In contrast, the symbolic V-function depicted in Figure 11, found by the SVI-SNGP method, has only 77 parameters.

D. Discussion

1) Performance of methods: The SPI and SVI methods are able to produce V-functions allowing to successfully solve the underlying control task (indicated by the maximum value of S equal to 100 %) for all the problems tested. They also clearly outperform the direct method. The best performance was
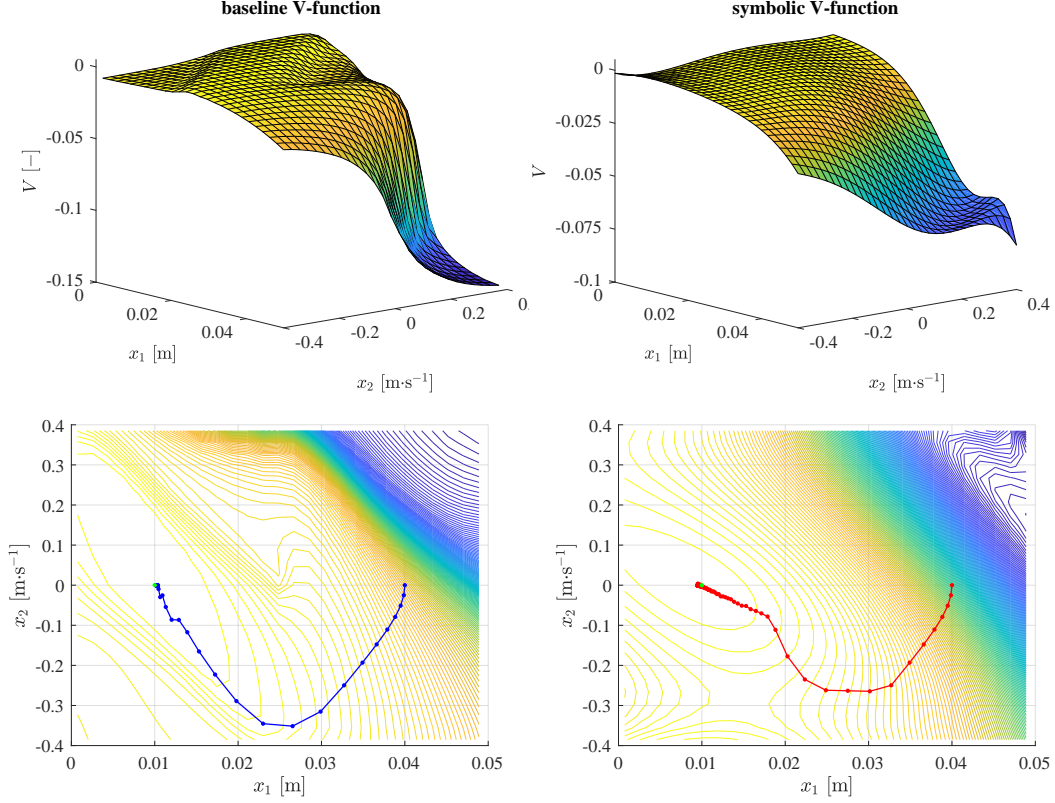
Fig. 11. Baseline and symbolic V-function produced by the `SVI-SNGP` method on the Magman problem. The symbolic V-function is smoother than the numerical baseline V-function and it performs the control task well. However, the way of approaching the goal state by using the symbolic V-function is inferior to the trajectory generated with the baseline V-function. This example illustrates the tradeoff between the complexity of the V-function and the ability of the algorithm to find those intricate details on the V-function surface that matter for the performance.

TABLE VII. EXPERIMENT PARAMETERS.

	Illustrative	1-DOF	2-DOF	Magman
State space dimensions	1	2	4	2
State space, $\mathcal{X}$	$[-10, 10]$	$[0, 2\pi] \times [-30, 30]$ $\times [-\pi, \pi] \times [-2\pi, 2\pi]$	$[-\pi, \pi] \times [-2\pi, 2\pi]$	$[0, 0.05] \times [-0.4, 0.4]$
Goal state, x_r	7	$[\pi\ 0]$	$[0\ 0\ 0\ 0]$	$[0.01\ 0]$
Input space dimensions	1	1	2	2
Input space, $\mathcal{U}$	$[-4, 4]$	$[-2, 2]$	$[-3, 3] \times [-1, 1]$	$[0, 0.6] \times [0, 0.6]$
# of control actions, n_u	41	11	9	25
Control actions set, U	$\{-4, -3.8, \ldots, 3.8, 4\}$	$\{-2, -1.6, -1.2, -0.8, -0.4,$ $0, 0.4, 0.8, 1.2, 1.6, 2\}$	$\{-3, 0, 3\} \times \{-1, 0, 1\}$	$\{0, 0.15, 0.3, 0.45, 0.6\} \times$ $\{0, 0.15, 0.3, 0.45, 0.6\}$
# of training samples, n_x	121	961	14641	729
Discount factor, γ	0.95	0.95	0.95	0.95
Sampling period, T_s [s]	0.001	0.05	0.01	0.01

TABLE VIII. SYMBOLIC REGRESSION PARAMETERS.

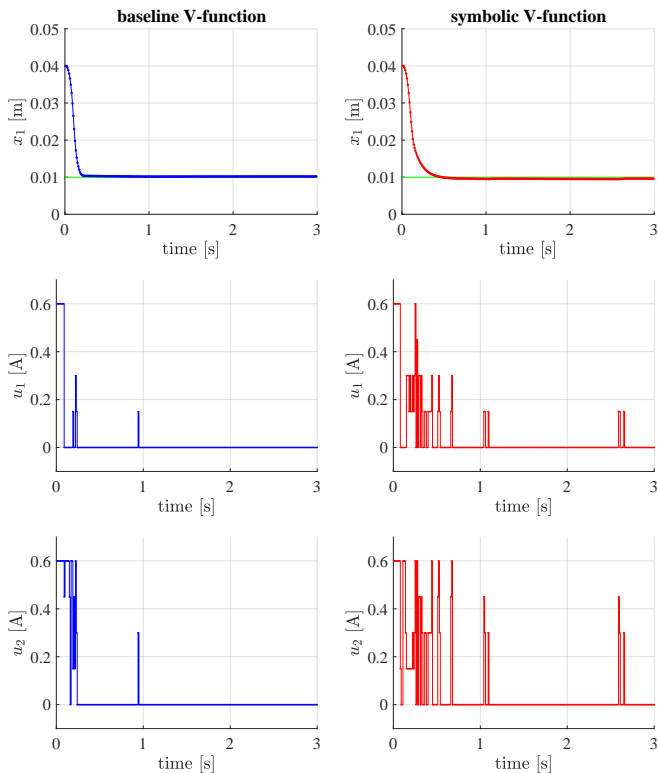|	Illustrative	1-DOF	2-DOF	Magman
Number of iterations, n_i	50 (30)	50 (30)	50 (30)	50 (30)
Number of runs, n_r	30	30	30	30
Simulation time, T_{sim}	1	5	10	3
Goal neighborhood, ε	0.05	$[0.1, 1]^{\top}$	$[0.1, 1, 0.1, 1]^{\top}$	$[0.001, 1]^{\top}$
Goal attainment end interval, T_{end}	0.01	2	2	1

Fig. 12. Simulations with the baseline V-function (left) and the symbolic V-function (right) found with the `SVI-SNGP` method on the Magman problem.

observed on the 1DOF problem (`SVI-SNGP` and `SVI-MGGP` generate 28 and 29 models with S=100 %, respectively) and the Magman (both `SPI-SNGP` and `SVI-SNGP` generate 30 models with S=100 %). The performance was significantly worse on the 2DOF problem (`SPI-MGGP` generated the best results with only 5 models with S=100 %). However, the performance of the successful value functions is much better than that of the baseline value function. The numerically approximated baseline V-function can only successfully control the system from 3 out of 13 initial states. This can be attributed to the rather sparse coverage of the state space since the approximator was constructed using a regular grid of $11 \times 11 \times 11 \times 11$ triangular basis functions.

Interestingly, the `direct` method implemented with SNGP was able to find several perfect V-functions with respect to S on the Magman. On the contrary, it completely failed to find such a V-function on the 2DOF and even on the 1DOF problem. We observed that although the 1DOF and Magman systems both had 2D state-space, the 1DOF problem is harder for the symbolic methods in the sense that the V-function has to be very precise at certain regions of the state space in order to allow for successful closed-loop control. This is not the case in the Magman problem, where V-functions that only roughly approximate the optimal V-function can perform well.

Overall, the two symbolic regression methods, SNGP and MGGP, performed equally well, although SNGP was slightly better on the 1DOF and Magman problem. Note, however, that

a thorough comparison of symbolic regression methods was not a primary goal of the experiments. We have also not tuned the control parameters of the algorithms at all and it is quite likely that if the parameters of the algorithms were optimized their performance would improve.

2) Number of parameters: One of the advantages of the proposed symbolic methods is the compactness of the value functions, which can be demonstrated, for instance, on the 1DOF problem. The symbolic value function found by using the `SVI-SNGP` method (Figure 6, right) has 100 free parameters, while the baseline numerically approximated value function has 961 free parameters. An alternative reinforcement learning approach uses neural networks in the actor-critic scheme. The critic is approximated by a shallow neural network [31] with 3791 parameters and by a deep network DDPG [9] with 122101 parameters. The symbolic value function achieves the same or better performance with orders of magnitude fewer parameters.

3) Computational complexity: The time needed for a single run of the `SVI`, `SPI` or `direct` method ranges from several minutes for the illustrative example to around 24 hours for the 2DOF problem on a standard desktop PC. The running time of the algorithm increases linearly with the size of the training data. However, the size of the training data set may grow exponentially with the state space dimension. In this article, we have generated the data on a regular grid. The efficiency gain depends on the way the data set is constructed. Other data generation methods are part of our future research. For high-dimensional problems, symbolic regression has the potential to be computationally more efficient than numerical approximation methods such as deep neural networks.

VI. CONCLUSIONS

We have proposed three methods based on symbolic regression to construct an analytic approximation of the V-function in a Markov decision process. The methods were experimentally evaluated on four nonlinear control problems: one first-order system, two second-order systems and one fourth-order system.

The main advantage of the approach proposed is that it produces smooth, compact V-functions, which are human-readable and mathematically tractable. The number of their parameters is an order of magnitude smaller than in the case of a basis function approximator and several orders of magnitude smaller than in (deep) neural networks. The control performance in simulations and in experiments on a real setup is excellent.

The most significant current limitation of the approach is its high computational complexity. However, as the dimensionality of the problem increases, numerical approximators starts to be limited by the computational power and memory capacity of standard computers. Symbolic regression does not suffer from such a limitation.

In our future work, we will evaluate the method on higher-dimensional problems, where we expect a large benefit over numerical approximators in terms of computational complexity. In relation to that, we will investigate smart methods for

generating the training data. We will also investigate the use of input–output models instead of state-space models and closed-loop stability analysis methods for symbolic value functions. We will also develop techniques to incrementally control the complexity of the symbolic value function depending on its performance.

REFERENCES

[1] R. Munos and A. Moore, "Variable resolution discretization in optimal control," *Machine learning*, vol. 49, no. 2, pp. 291–323, 2002.

[2] L. Buşoniu, D. Ernst, B. De Schutter, and R. Babuška, "Cross-entropy optimization of control policies with adaptive basis functions," *IEEE Transactions on Systems, Man, and Cybernetics—Part B: Cybernetics*, vol. 41, no. 1, pp. 196–209, 2011.

[3] D. Ernst, P. Geurts, and L. Wehenkel, "Tree-based batch mode reinforcement learning," *Journal of Machine Learning Research*, vol. 6, pp. 503–556, 2005.

[4] C. G. Atkeson, A. W. Moore, and S. Schaal, "Locally weighted learning," *Artificial Intelligence Review*, vol. 11, no. 1-5, pp. 11–73, 1997.

[5] I. Grondman, M. Vaandrager, L. Buşoniu, R. Babuška, and E. Schuitema, "Efficient model learning methods for actor–critic control," *IEEE Transactions on Systems, Man, and Cybernetics, Part B: Cybernetics*, vol. 42, no. 3, pp. 591–602, 2012.

[6] S. Lange, M. Riedmiller, and A. Voigtlander, "Autonomous reinforcement learning on raw visual input data in a real world application," in *Proceedings 2012 International Joint Conference on Neural Networks (IJCNN)*, Brisbane, Australia, June 2012, pp. 1–8.

[7] V. Mnih, K. Kavukcuoglu, D. Silver, A. Graves, I. Antonoglou, D. Wierstra, and M. Riedmiller, "Playing atari with deep reinforcement learning," vol. arxiv.org/abs/1312.5602, 2013.

[8] V. Mnih, K. Kavukcuoglu, D. Silver, A. A. Rusu, J. Veness, M. G. Bellemare, A. Graves, M. Riedmiller, A. K. Fidjeland, G. Ostrovski, S. Petersen, C. Beattie, A. Sadik, I. Antonoglou, H. King, D. Kumaran, D. Wierstra, S. Legg, and D. Hassabis, "Human-level control through deep reinforcement learning," *Nature*, vol. 518, no. 7540, pp. 529–533, 2015.

[9] T. P. Lillicrap, J. J. Hunt, A. Pritzel, N. Heess, T. Erez, Y. Tassa, D. Silver, and D. Wierstra, "Continuous control with deep reinforcement learning," *CoRR*, vol. abs/1509.02971, 2015. [Online]. Available: http://arxiv.org/abs/1509.02971

[10] T. de Bruin, J. Kober, K. Tuyls, and R. Babuška, "Off-policy experience retention for deep actor-critic learning," in *Deep Reinforcement Learning Workshop, Advances in Neural Information Processing Systems (NIPS)*, 2016.

[11] P. Nagarajan and G. Warnell, "The impact of nondeterminism on reproducibility in deep reinforcement learning," 2018.

[12] E. Alibekov, J. Kubalík, and R. Babuška, "Policy derivation methods for critic-only reinforcement learning in continuous action spaces," *Engineering Applications of Artificial Intelligence*, 2018.

[13] M. Schmidt and H. Lipson, "Distilling free-form natural laws from experimental data," *Science*, vol. 324, no. 5923, pp. 81–85, 2009.

[14] E. Vladislavleva, T. Friedrich, F. Neumann, and M. Wagner, "Predicting the energy output of wind farms based on weather data: Important variables and their correlation," *Renewable Energy*, vol. 50, pp. 236–243, 2013.

[15] N. Staelens, D. Deschrijver, E. Vladislavleva, B. Vermeulen, T. Dhaene, and P. Demeester, "Constructing a No-Reference H. 264/AVC Bitstream-based Video Quality Metric using Genetic Programming-based Symbolic Regression," *Circuits and Systems for Video Technology, IEEE Transactions on*, vol. 99, pp. 1–12, 2012.

[16] C. Brauer, "Using Eureqa in a Stock Day-Trading Application," 2012, cypress Point Technologies, LLC.

[17] M. Onderwater, S. Bhulai, and R. van der Mei, "Value function discovery in markov decision processes with evolutionary algorithms," *IEEE Transactions on Systems, Man, and Cybernetics: Systems*, vol. 46, no. 9, pp. 1190–1201, Sept 2016.

[18] M. Davarynejad, J. van Ast, J. Vrancken, and J. van den Berg, "Evolutionary value function approximation," in *Adaptive Dynamic Programming And Reinforcement Learning (ADPRL), 2011 IEEE Symposium on*. IEEE, 2011, pp. 151–155.

[19] D. Jackson, *A New, Node-Focused Model for Genetic Programming*. Berlin, Heidelberg: Springer, 2012, pp. 49–60.

[20] ——, *Single Node Genetic Programming on Problems with Side Effects*. Berlin, Heidelberg: Springer, 2012, pp. 327–336.

[21] E. Alibekov, J. Kubalík, and R. Babuška, "Symbolic method for deriving policy in reinforcement learning," in *Proceedings 55th IEEE Conference on Decision and Control (CDC)*, Las Vegas, USA, Dec. 2016, pp. 2789–2795.

[22] J. Kubalík, E. Derner, and R. Babuška, "Enhanced symbolic regression through local variable transformations," in *Proceedings 9th International Joint Conference on Computational Intelligence (IJCCI 2017)*, Madeira, Portugal, Nov. 2017, pp. 91–100.

[23] M. Hinchliffe, H. Hiden, B. McKay, M. Willis, M. Tham, and G. Barton, "Modelling chemical process systems using a multi-gene genetic programming algorithm," in *Late Breaking Paper, GP'96*, Stanford, USA, 1996, pp. 56–65.

[24] D. P. Searson, "GPTIPS 2: An open-source software platform for symbolic data mining," in *Handbook of Genetic Programming Applications*. Springer International Publishing, 2015, pp. 551–573. [Online]. Available: https://doi.org/10.1007/978-3-319-20883-1_22

[25] J. Žegklitz and P. Pošík, "Linear combinations of features as leaf nodes in symbolic regression," in *Proceedings of the Genetic and Evolutionary Computation Conference Companion*, ser. GECCO '17. New York, NY, USA: ACM, 2017, pp. 145–146. [Online]. Available: http://doi.acm.org/10.1145/3067695.3076009

[26] I. Arnaldo, K. Krawiec, and U.-M. O'Reilly, "Multiple regression genetic programming," in *Proceedings of the 2014 Annual Conference on Genetic and Evolutionary Computation*, ser. GECCO '14. New York, NY, USA: ACM, 2014, pp. 879–886. [Online]. Available: http://doi.acm.org/10.1145/2576768.2598291

[27] I. Arnaldo, U.-M. O'Reilly, and K. Veeramachaneni, "Building predictive models via feature synthesis," in *Proceedings of the 2015 Annual Conference on Genetic and Evolutionary Computation*, ser. GECCO '15. New York, NY, USA: ACM, 2015, pp. 983–990. [Online]. Available: http://doi.acm.org/10.1145/2739480.2754693

[28] R. Sutton and A. Barto, *Reinforcement learning: An introduction*. Cambridge Univ Press, 1998, vol. 1, no. 1.

[29] L. Busoniu, R. Babuska, B. De Schutter, and D. Ernst, *Reinforcement learning and dynamic programming using function approximators*. CRC PressI Llc, 2010, vol. 39.

[30] K. Verbert, R. Tóth, and R. Babuška, "Adaptive friction compensation: A globally stable approach," *IEEE/ASME Transactions on Mechatronics*, vol. 21, no. 1, pp. 351–363, 2016.

[31] T. de Bruin, J. Kober, K. Tuyls, and R. Babuška, "Experience selection in deep reinforcement learning for control," *Journal of Machine Learning Research*, 2018.

[32] J. Damsteeg, S. Nageshrao, and R. Babuška, "Model-based real-time control of a magnetic manipulator system," in *Proceedings 56th IEEE Conference on Decision and Control (CDC)*, Melbourne, Australia, Dec. 2017, pp. 3277–3282.